



## OPEN Role of $P_2 \times_7$ receptor during focused ultrasound induced blood brain barrier modulation

Junwon Park<sup>1,5</sup>, Young Cheol Na<sup>1,2,5</sup>, Jihyeon Lee<sup>3</sup>, Younghee Seo<sup>1</sup>, Hojin Kim<sup>4</sup>, Sangheon Han<sup>1</sup>, Byeong-Wook Song<sup>4</sup>✉ & Won Seok Chang<sup>1</sup>✉

Although low-intensity focused ultrasound (LiFUS) with microbubbles is used to temporally open the blood-brain barrier (BBB), the underlying mechanism is not fully understood. This study aimed to analyze BBB-related alterations in the brain microenvironment after LiFUS, with a focus on the involvement of the purinergic  $P_2 \times_7$  receptor. Sprague-Dawley rats were sonicated with LiFUS at 0.3 MPa energy. The impact of LiFUS on the  $P_2 \times_7$  receptor and inflammatory-related proteins, including NLRP3 and interleukin-1 $\beta$ , was analyzed through western blotting. The BBB-associated tight junction proteins, zonula occludens-1 (ZO-1) and occludin, were also analyzed. BBB permeability was assessed by quantifying the amount of Evans blue dye penetration using spectrophotometry. Furthermore, the safety of the sonication procedure was verified via terminal deoxynucleotidyl transferase dUTP nick end labeling (TUNEL) assay and hematoxylin and eosin staining. Substantial increases in the  $P_2 \times_7$  receptor and its downstream signaling were confirmed after sonicating the BBB with LiFUS for 1 h ( $p < 0.05$ ). Conversely, for tight junction proteins, the lowest expression was observed at 1 h ( $p < 0.001$ ). Both responses were normalized back to the original state over time. No evidence of brain damage was observed during the procedure. Furthermore, the  $P_2 \times_7$  receptor antagonist-injected group showed reduced Evans blue dye penetration compared to that 1 h after FUS, indicating a mitigated impact of LiFUS on the BBB. Herein, we elucidate the underlying mechanism by which LiFUS affects the BBB, with a focus on the involvement of the  $P_2 \times_7$  receptor. Our findings demonstrate that the extent of BBB opening varies upon the regulation of the  $P_2 \times_7$  receptor. This study provides valuable insights into the mechanisms underlying BBB modulation through LiFUS, thereby laying the foundation for expanding its applications.

The blood brain barrier (BBB) is a complex structure that plays a crucial role in maintaining homeostasis within the central nervous system (CNS)<sup>1</sup>. The BBB consists of endothelial cells with tight junctions, basal lamina, end-feet of astrocytes, and pericytes embedded in the basement membrane<sup>2,3</sup>. This distinctive arrangement gives the brain immune privilege, while simultaneously presenting a tremendous challenge for the treatment of brain diseases<sup>4,5</sup>. Numerous attempts have been made to facilitate efficient drug penetration through the BBB; however, an optimized approach is yet to be established<sup>6,7</sup>.

Low-intensity focused ultrasound (LiFUS) with microbubbles has emerged as a promising technique<sup>8,9</sup>. Moreover, high-intensity focused ultrasound for the thermal coagulation of tissues has been applied, particularly for the treatment of patients with essential tremors<sup>10,11</sup>. These pioneering techniques serve as a foundation for expanding the concept of using ultrasound in the field of neuroscience, specifically in relation to the brain<sup>12,13</sup>. Unlike conventional clinical applications of focused ultrasound, LiFUS induces the oscillation of microbubbles with a relatively small amount of energy<sup>14</sup>. Many studies have reported that the cavitation effect of bubbles causes loosening of the tight junctions between endothelial cells, leading to a noninvasive, transient, and localized opening of the BBB<sup>15</sup>. Extensive studies have been conducted to investigate the potential of LiFUS for modulating the BBB. Several studies have analyzed the stability of LiFUS using various parameters<sup>16–18</sup>. Other, drug delivery studies have targeted neurodegenerative diseases such as Parkinson's disease and Alzheimer's disease<sup>19–22</sup>. Furthermore, considerable efforts have been made to investigate alterations in the brain microenvironment following the sonication procedure<sup>23–26</sup>. In particular, many studies have evaluated the safety aspects and

<sup>1</sup>Department of Neurosurgery and Brain Research Institute, Yonsei University College of Medicine, Seoul, Republic of Korea. <sup>2</sup>Department of Neurosurgery, Catholic Kwandong University College of Medicine, International St Mary's Hospital, Incheon Metropolitan City, Republic of Korea. <sup>3</sup>Cleros Biotech, Seoul, Korea. <sup>4</sup>Department of Medical Science, College of Medicine, Catholic Kwandong University, Gangneung-si, Gangwon-do, Republic of Korea. <sup>5</sup>Junwon Park and Young Cheol Na contributed equally. ✉email: songbw@cku.ac.kr; changws0716@yuhs.ac

inflammatory responses after LiFUS<sup>27–29</sup>. However, the molecular mechanisms underlying LiFUS-induced BBB modulation are not fully understood, particularly the primary factors driving this process<sup>30,31</sup>.

Once external stress occurs in the brain, the primary response is an increase in extracellular adenosine triphosphate (ATP)<sup>32</sup>. This ATP increase leads to the activation of purinergic receptors, of which the  $P_2 \times_7$  receptor is considered one of the main members<sup>33</sup>.  $P_2 \times_7$  receptors are ATP-gated ion channels that are widely expressed in various components of neurovascular units, including neurons, oligodendrocytes, microglia, and endothelial cells<sup>33,34</sup>. These receptors have been implicated in a broad range of physiological and pathological processes, including inflammation, apoptosis, and cell death<sup>35–37</sup>. Owing to their distinctive characteristics,  $P_2 \times_7$  receptors have been mainly investigated in neurodegenerative diseases and tumors, focusing on their involvement in inflammatory responses<sup>38,39</sup>. Recently, a few studies have demonstrated that the regulation of  $P_2 \times_7$  receptors can protect against BBB breakdown induced by lipopolysaccharide and mitigate the damage caused by alcohol and nicotine exposure<sup>40–42</sup>. In addition, the expression levels of tight junction proteins, such as claudin-5 and occluding, were preserved in animal stroke models by regulating the  $P_2 \times_7$  receptor<sup>43</sup>. These findings highlight the significant effect of  $P_2 \times_7$  receptors on BBB permeability<sup>44</sup>. Gradual upregulation of the mRNA expression of  $P_2 \times_7$  receptors was observed in an osteoblast model following LiFUS<sup>45</sup>. Although this study did not include an in vivo experiment, it showed the potential of LiFUS in modulating the expression of the  $P_2 \times_7$  receptor<sup>45</sup>.

This study aimed to analyze BBB-related alterations in the brain microenvironment after LiFUS, with a focus on the involvement of the purinergic  $P_2 \times_7$  receptor. Based on the previous results, we hypothesized that BBB modulation induced by LiFUS might be related to the  $P_2 \times_7$  receptor and analyzed the factors associated with  $P_2 \times_7$  receptors and their potential roles in BBB modulation.

## Results

### Confirmation of BBB opening after LiFUS

First, the sonication area of LiFUS and the degree of BBB opening were confirmed. Prior to the analysis of the  $P_2 \times_7$  receptor, LiFUS with microbubbles was used to identify the area of the lesion and analyze the changes in MRI signals (Fig. 1a and b). The results confirmed that the energy reached part of the upper layer of the thalamus (DV: 4 mm from the bregma), including the hippocampus, through the T1-contrast-enhanced image. In addition, by quantifying the intensity of the ipsilateral and contralateral signals using the same ROI, it was found that the signals of the sonicated area (LiFUS:  $215.6 \pm 37.3$ ) were significantly enhanced (Con:  $115.8 \pm 39.3$ ,  $p < 0.05$ ,  $n = 3$  for each group).

### Alterations in $P_2 \times_7$ receptor expression and signaling cascade following LiFUS

To investigate whether ultrasound energy affects the  $P_2 \times_7$  receptor, we initially employed immunohistochemistry (IHC) to assess the variations in receptor expression levels over time (Fig. 2a). A notable upregulation of receptor expression in the hippocampus within the group 1 h after LiFUS. For a more accurate quantitative analysis, we conducted western blotting and real-time RT-PCR to evaluate the protein and RNA expression levels of the  $P_2 \times_7$  receptor. A significant increase in protein expression was observed in the group 1 h (1 h:  $155.9 \pm 34.5$ ) after sonication compared to that in the other groups (Fig. 2b, Con:  $100 \pm 12.4$ ,  $p < 0.05$ ; 4 h:  $98.9 \pm 32$ ,  $p < 0.05$ ; 24 h:  $98.3 \pm 41.8$ ,  $p < 0.05$ ,  $n = 5$  for each group). Similarly, the RNA levels showed a significant increase in the group corresponding to 1 h after LiFUS (1 h:  $233.9 \pm 20$ ) compared to the other groups (Fig. 2c, Con:  $100 \pm 14.8$ ,  $p < 0.001$ ; 4 h:  $165.6 \pm 22.3$ ,  $p < 0.001$ ; 24 h:  $139.7 \pm 17.9$ ,  $p < 0.001$ ,  $n = 5$  for each group). Notably, the RNA expression levels remained elevated even after 24 h (4 h:  $p < 0.001$ ; 24 h:  $p < 0.05$ , compared to the Con).

We also analyzed NLRP3 and IL-1 $\beta$  levels, which are known to exhibit a substantial correlation with  $P_2 \times_7$  receptor expression<sup>32</sup>. The protein expression pattern of NLRP3 was similar to that of the  $P_2 \times_7$  receptor, peaking at 1 h after LiFUS (1 h:  $188.7 \pm 28.9$ ), but with a slight difference in the significance among groups

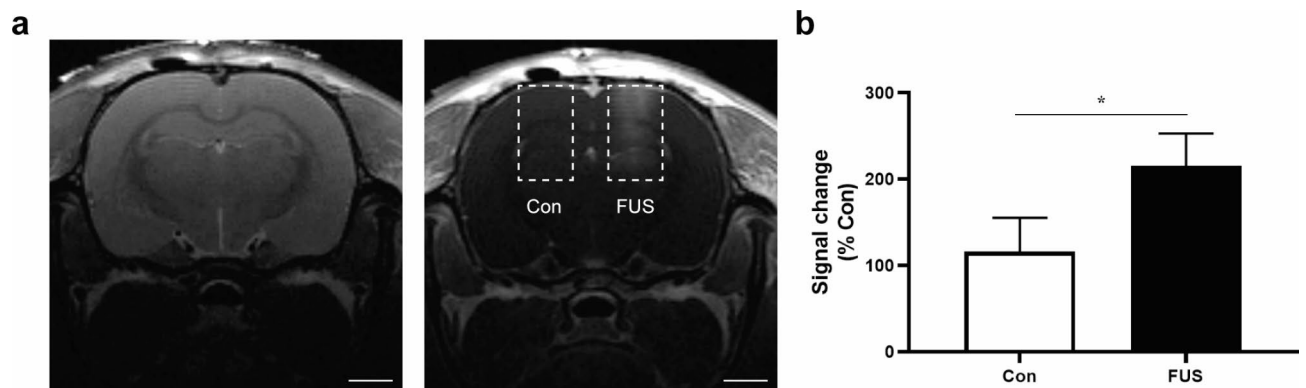


**Fig. 1.** Signal alteration after LiFUS in MRI images. **(a)** Representative MR images to confirm the opening of the BBB. T2-weighted images (left) and T1-weighted images (right) were used. The opening of the BBB (white box, with LiFUS) can be seen compared to the opposite. Scale bar: 2.5 mm. **(b)** The enhanced signal in the ROI after LiFUS. All data are represented as the mean  $\pm$  SD ( $n = 3$ ). Unpaired t-test was performed; \* $p < 0.05$  compared to the Con.

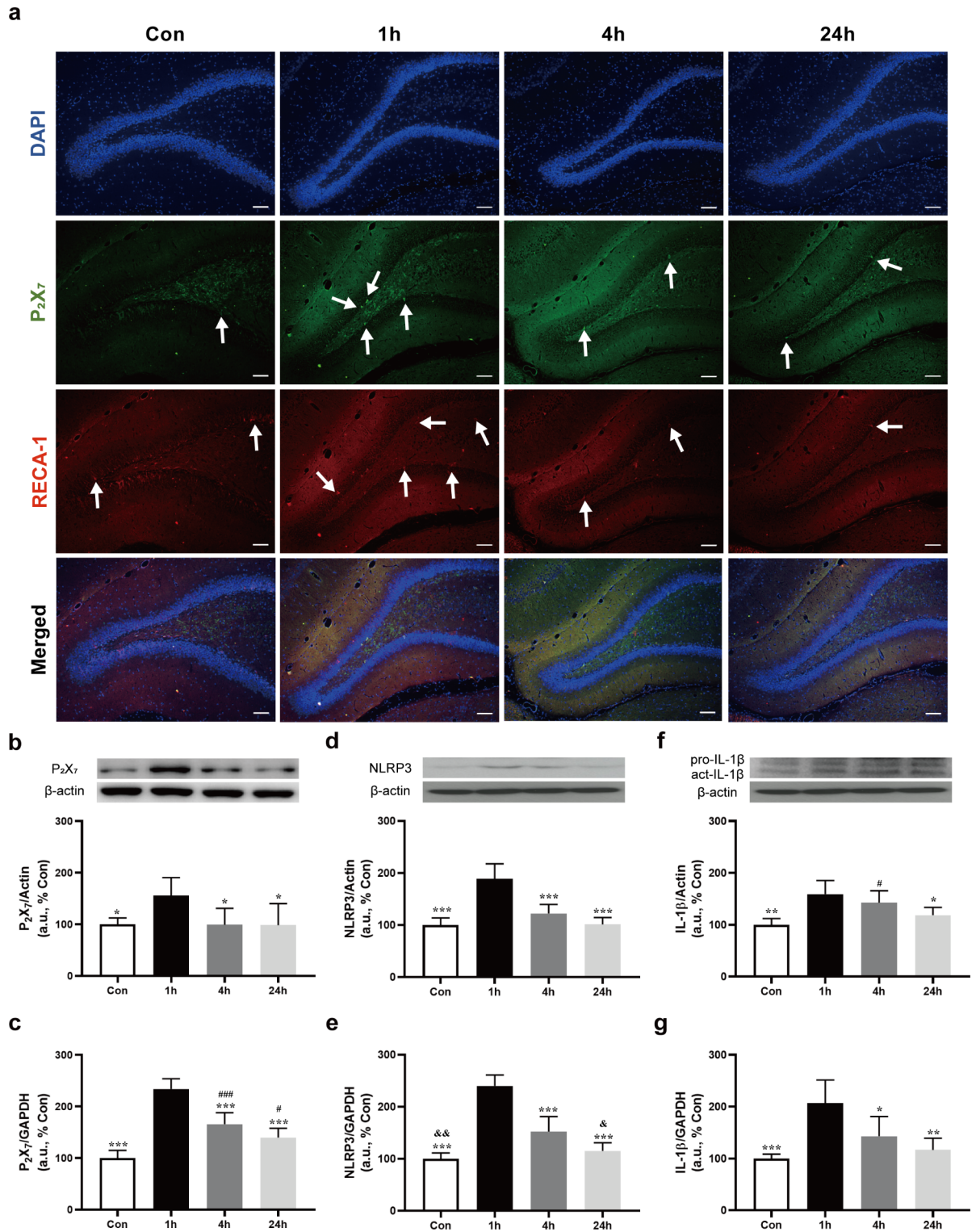


**Fig. 2.** Regulation of P<sub>2</sub>X<sub>7</sub>-receptors and downstream signaling pathways after sonication. **(a)** Representative IHC images of DAPI (blue), P<sub>2</sub>X<sub>7</sub> receptor (white arrow, green) and RECA-1 (white arrow, red) in the hippocampal region of the brain after LiFUS. Scale bar: 100 μm. **(b,c)** Western blotting and RT-PCR results for P<sub>2</sub>X<sub>7</sub> receptors. The bar graph shows the normalized level of the receptors relative to the control. Band intensity images for each group are also included. \*  $p < 0.05$ , \*\*  $p < 0.01$ , \*\*\*  $p < 0.001$ ; compared to 1 h, #  $p < 0.05$ , ###  $p < 0.001$ ; compared to Con. **(d,e)** Western blot and RT-PCR results for NLRP3 inflammasome. The analysis method employed for NLRP3 was the same as that for the P<sub>2</sub>X<sub>7</sub> receptors. \*\*  $p < 0.01$ , \*\*\*  $p < 0.001$ ; compared to 1 h, &  $p < 0.05$ , &&  $p < 0.01$ ; compared to 4 h. **(f,g)** Western blot and RT-PCR results for IL-1β. The analysis method employed for NLRP3 was the same as that for the P<sub>2</sub>X<sub>7</sub> receptors. \*  $p < 0.05$ , \*\*  $p < 0.01$ , \*\*\*  $p < 0.001$ ; compared to 1 h, #  $p < 0.05$ ; compared to Con. All data are represented as mean ± SD ( $n = 5$ ). One-way ANOVA with Tukey's multiple comparison test was performed.



(Fig. 2d, Con:  $100 \pm 13.7$ ,  $p < 0.001$ ; 4 h:  $122.4 \pm 17.1$ ,  $p < 0.001$ ; 24 h:  $101.2 \pm 13.2$ ,  $p < 0.001$ ,  $n = 5$  for each group). Similar results were obtained with the RNA levels (Fig. 2e, Con:  $100 \pm 11.12$ ,  $p < 0.001$ ; 4 h:  $152.2 \pm 28.9$ ,  $p < 0.001$ ; 24 h:  $114.9 \pm 15.7$ ,  $p < 0.001$  compared to 1 h:  $239.8 \pm 21.2$ ,  $n = 5$  for each group). However, NLRP3 RNA levels remained elevated until 4 h after LiFUS (Con:  $p < 0.01$ ; 24 h:  $p < 0.05$  compared to 4 h). IL-1 $\beta$  protein expression level showed similar trends (Fig. 2f, Con:  $100 \pm 11.8$ ,  $p < 0.01$ ; 4 h:  $142.7 \pm 22.9$ ; 24 h:  $118.6 \pm 14.9$ ,  $p < 0.05$  compared to the 1 h:  $159.2 \pm 26.2$ ,  $n = 5$  for each group). The protein levels were found to be upregulated for up to 4 h compared to those in the control group ( $p < 0.05$ ). In terms of RNA expression, the highest peak was observed at 1 h after sonication (Fig. 2g, Con:  $100 \pm 8.5$ ,  $p < 0.001$ ; 4 h:  $142.8 \pm 38.2$ ,  $p < 0.05$ ; 24 h:  $116.5 \pm 22.6$ ,  $p < 0.01$  compared to 1 h:  $206.9 \pm 44.4$ ,  $n = 5$  for each group). Taken together, these results showed the upregulation of the receptor and its signaling after LiFUS treatment, with the expression levels gradually returning to baseline within a day. The findings suggest that LiFUS temporally affects the P<sub>2</sub>×<sub>7</sub> receptor and related proinflammatory cytokines.

### Alterations of BBB-related protein expression after LiFUS

We assessed alterations in BBB-related proteins, such as ZO-1 and occludin, to confirm the impact of LiFUS on BBB integrity using western blotting and RT-PCR. Initially, ZO-1 exhibited the lowest protein expression at 1 h after sonication (1 h:  $57.4 \pm 12.5$ ,  $p < 0.01$  compared to Con), in contrast to the P<sub>2</sub>×<sub>7</sub> receptor, after which ZO-1 protein expression gradually normalized over time (Fig. 3a, Con:  $100 \pm 11.2$ ; 4 h:  $71.2 \pm 16.5$ ,  $p < 0.05$  compared to Con; 24 h:  $119 \pm 17.2$ ). The reduced expression level remained significant in the group a day after sonication (1 h and 4 h:  $p < 0.001$  compared to 24 h). This trend was consistent at the ZO-1 RNA level (Fig. 3b, Con:  $100 \pm 10.9$ ; 1 h:  $41.4 \pm 8.3$ ,  $p < 0.001$  compared to Con and 24 h; 4 h:  $69.2 \pm 10.3$ ,  $p < 0.001$  compared to 24 h; 24 h:  $126.8 \pm 32.5$ ). Occludin, a representative tight junction protein, exhibited similar patterns in both protein and RNA levels (Fig. 3c and d, occludin protein expression: Con:  $100 \pm 9.7$ ; 1 h:  $44.5 \pm 9.7$ ,  $p < 0.001$  compared to con and 24 h; 4 h:  $59.7 \pm 18.1$ ,  $p < 0.001$  compared to Con and 24 h; 24 h:  $112 \pm 12.2$  and occludin RNA expression: Con:  $100 \pm 12.6$ ; 1 h:  $39 \pm 10.1$ ,  $p < 0.01$  compared to con and  $p < 0.001$  compared to 24 h; 4 h:  $55.3 \pm 14.4$ ,  $p < 0.05$  compared to Con and  $p < 0.001$  compared to Con and 24 h; 24 h:  $117.3 \pm 34.1$ ). In addition, MMP9, which is reportedly correlated to the BBB<sup>46</sup>, was observed through IHC, and its expression was partially elevated at after LiFUS even after 24 h (Fig. 3e). In addition, the expression of MMP2 data for each time point is shown in Fig. S1. These findings indicate that LiFUS influences BBB integrity and enhances BBB permeability. However, this effect may be transient, as BBB permeability returns to normal within a day.

### Safety assessment of LiFUS-induced BBB modulation

After confirming that ultrasound energy was sufficient for BBB modulation, we conducted a comprehensive safety assessment of the process. Initially, we monitored the ATP levels over time following LiFUS treatment (Fig. 4a). Consistent with previous findings, the highest concentration of ATP was found at 1 h after LiFUS (1 h:  $143.9 \pm 1.89$ ,  $p < 0.001$  compared to Con), with continued elevation even after 24 h (con:  $100 \pm 9.18$ ; 4 h:  $131.4 \pm 9.73$ ,  $p < 0.01$ ; 24 h:  $120.9 \pm 7.43$ ,  $p < 0.05$  compared to Con,  $n = 5$  for each group). Subsequently, we conducted an analysis of alterations in the NF- $\kappa$ B expression levels in response to the observed temporal increase in IL-1 $\beta$ . Thus, NF- $\kappa$ B expression levels may represent a signal transduction outcome of P<sub>2</sub>×<sub>7</sub> receptor activation after LiFUS. These findings are consistent with our prior data. Specifically, there was a noticeable elevation in the expression of phosphorylated NF- $\kappa$ B (p-NF- $\kappa$ B) within 1 h (Figs. 1h and 4b:  $312.1 \pm 74.8$ ). Additionally, their results gradually returned to baseline over time (p-NF- $\kappa$ B, Con:  $100 \pm 33$ ; 4 h:  $118.5 \pm 31.1$ ; 24 h:  $117.5 \pm 48.8$ ,  $p < 0.001$  compared to 1 h,  $n = 5$  for each group).

Subsequently, a comprehensive analysis of the cellular damage and apoptosis resulting from sonication was performed. Quantification of the RNA expression levels of caspase 3/9, used as markers of apoptosis, revealed an increased expression level 1 h post-sonication (Fig. 4c and d). However, this increase did not show statistical significance, and caspase 3/9 expression subsequently returned to baseline levels (caspase 3; Con:  $100 \pm 19$ ; 1 h:  $136.3 \pm 39.6$ ; 4 h:  $144.4 \pm 50.4$ ; 24 h:  $135.9 \pm 38.8$ , caspase 9; Con:  $100 \pm 9.8$ ; 1 h:  $123.8 \pm 28.9$ ; 4 h:  $126.8 \pm 27.2$ ; 24 h:  $113.3 \pm 22.4$ ,  $n = 5$  for each group). Although TUNEL assay results indicated some of activated cell death signals in 1 and 4 h, it normalized within a day (Fig. 4e). Finally, histopathological examination (H&E staining) confirmed the absence of tissue damage following LiFUS, which was consistent with the findings of the control group. The complete set of whole-brain tissue data for each time point is shown in Fig. S2. Collectively, these results highlight the ability of LiFUS to modulate BBB permeability without inducing brain damage, even in the context of P<sub>2</sub>×<sub>7</sub> receptor activation and transient upregulation of pro-inflammatory cytokines.

### Decreased BBB permeability after P<sub>2</sub>×<sub>7</sub> receptor antagonist injection

To substantiate the involvement of P<sub>2</sub>×<sub>7</sub> receptors in LiFUS-induced BBB opening, quantitative analysis of Evans blue was performed using spectrometry<sup>47</sup> (Fig. 5a). The groups used in this study were as follows: Con, Con + A438079, 1 h, 1 h + A438079, 4 h, 4 h + A438079, 24 h, and 24 h + A438079 ( $n = 5$  for each group). The group that received Evans blue administration at 1 h after sonication (1 h:  $0.051 \pm 0.01$ ) exhibited a significantly higher fluorescence intensity compared to that in all the other groups, except the group corresponding to 1 h + A438079 (Fig. 5b, Con:  $0.038 \pm 0.001$ ,  $p < 0.001$ ; Con + A438079:  $0.038 \pm 0.001$ ,  $p < 0.001$ ; 1 h + A438079:  $0.043 \pm 0.002$ ; 4 h:  $0.039 \pm 0.002$ ,  $p < 0.01$ ; 4 h + A438079:  $0.038 \pm 0.002$ ,  $p < 0.001$ ; 24 h:  $0.039 \pm 0.002$ ,  $p < 0.001$ ; 24 h + A438079:  $0.038 \pm 0.001$ ,  $p < 0.001$  compared to 1 h). Similarly, upon antagonist administration, the extent of leakage was most pronounced in the 1-hour post-LiFUS group; however, this result was not statistically significant when compared to the control. Notably, the amount of leakage was comparable to that observed in the group that received Evans blue at 4 h after LiFUS.



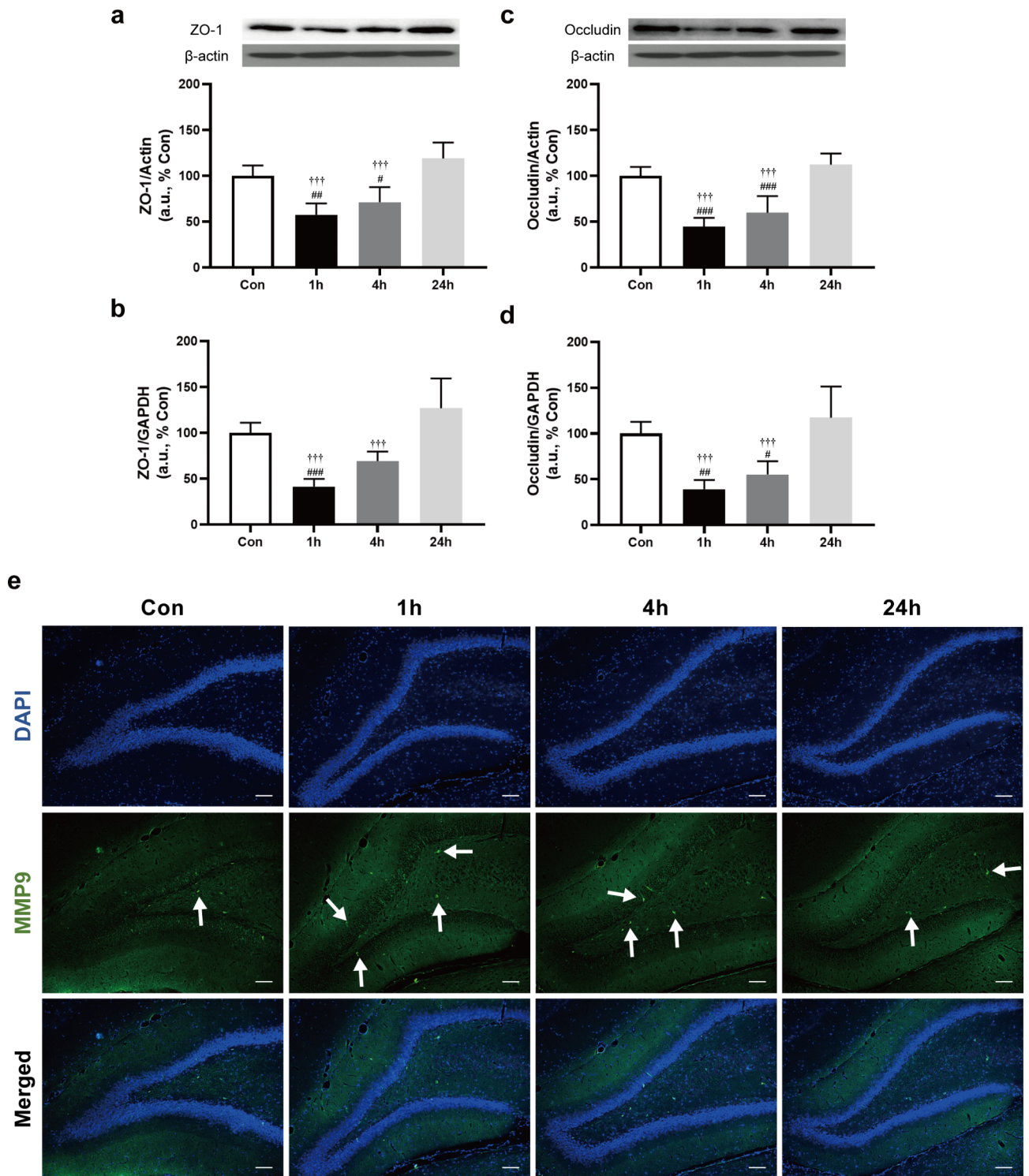


**Fig. 3.** Regulation of BBB-related proteins after LiFUS stimulation. **(a,b)** Western blot and RT-PCR results for ZO-1. The bar graph shows the normalized level of the receptors relative to that of control. Band intensity images for each group are included. #  $p < 0.05$ , ##  $p < 0.01$ , ###  $p < 0.001$ ; compared to Con, †††  $p < 0.001$ ; compared to 24 h. **(c,d)** Western blot and RT-PCR results for occludin. The analysis method employed for occludin was the same as that for ZO-1. #  $p < 0.05$ , ##  $p < 0.01$ , ###  $p < 0.001$ ; compared to Con, †††  $p < 0.001$ ; compared to 24 h. All data are presented as mean  $\pm$  SD ( $n = 5$ ). One-way ANOVA with Tukey's multiple comparison test was performed. **(e)** Representative IHC images of DAPI (blue) and MMP-9 (white arrow, green) in the hippocampal region of the brain after LiFUS. Scale bar: 100  $\mu$ m.

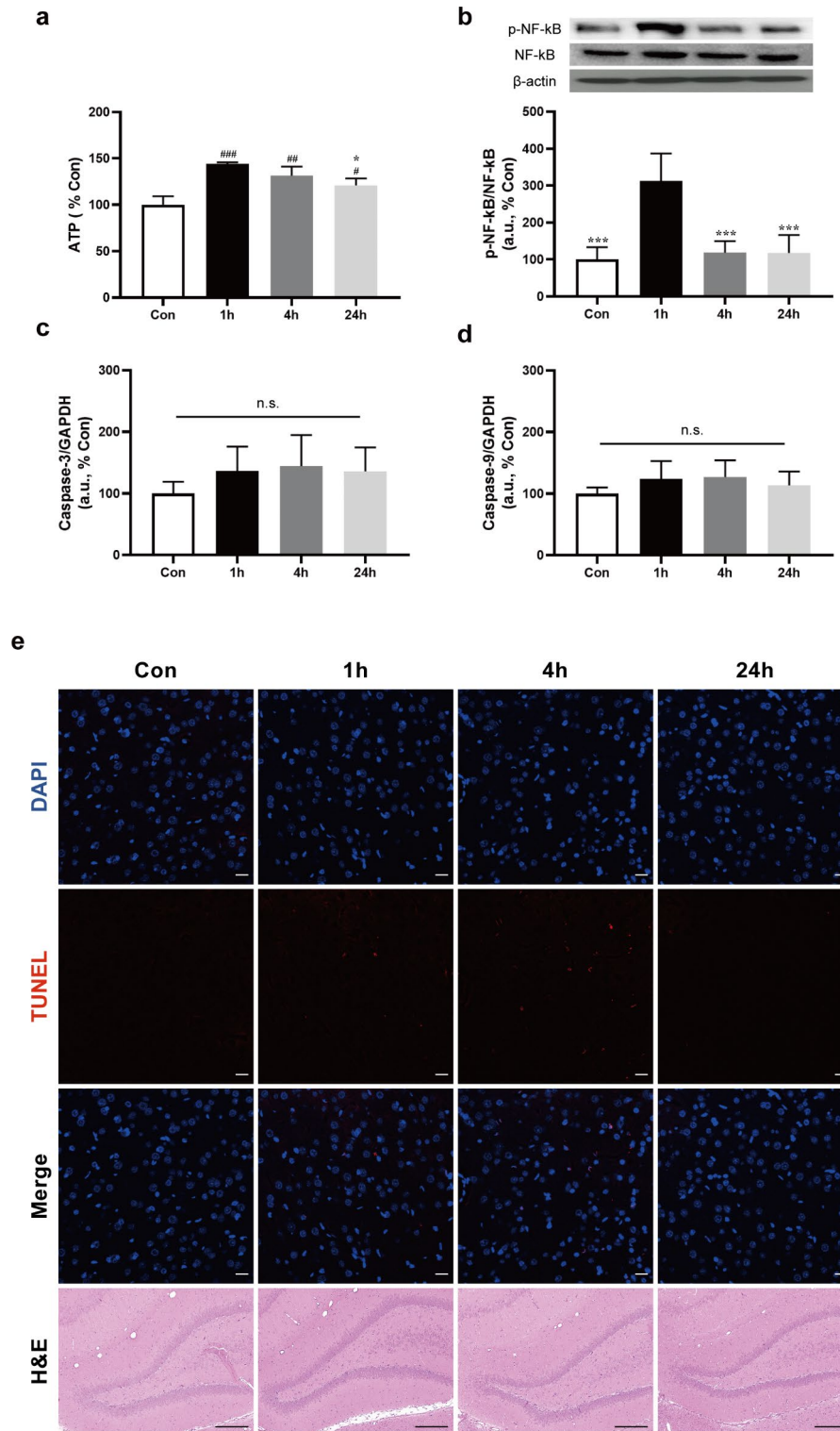


**Fig. 4.** No evidence of death signals after LiFUS stimulation. **(a)** Results of ATP quantification in the lesion. The bar graph shows the normalized level of ATP relative to that of control. #  $p < 0.05$ , ##  $p < 0.01$ , ###  $p < 0.001$ ; compared to Con, \*  $p < 0.05$ ; compared to 1 h. **(b)** Western blot results for NF- $\kappa$ B. The bar graph shows the normalized level of the receptor relative to that of the control. Band intensity images for each group are included. \*\*\*  $p < 0.001$ ; compared to 1 h. **(c,d)** RT-PCR results for caspase 3/9. No significant differences were observed among the groups. All data are represented as mean  $\pm$  SD ( $n = 5$ ). One-way ANOVA with Tukey's multiple comparison test was performed. **(e)** Representative images of the TUNEL assay (white arrow) and H&E images of each group. Scale bar: 20  $\mu$ m for TUNEL and 100  $\mu$ m for H&E images.

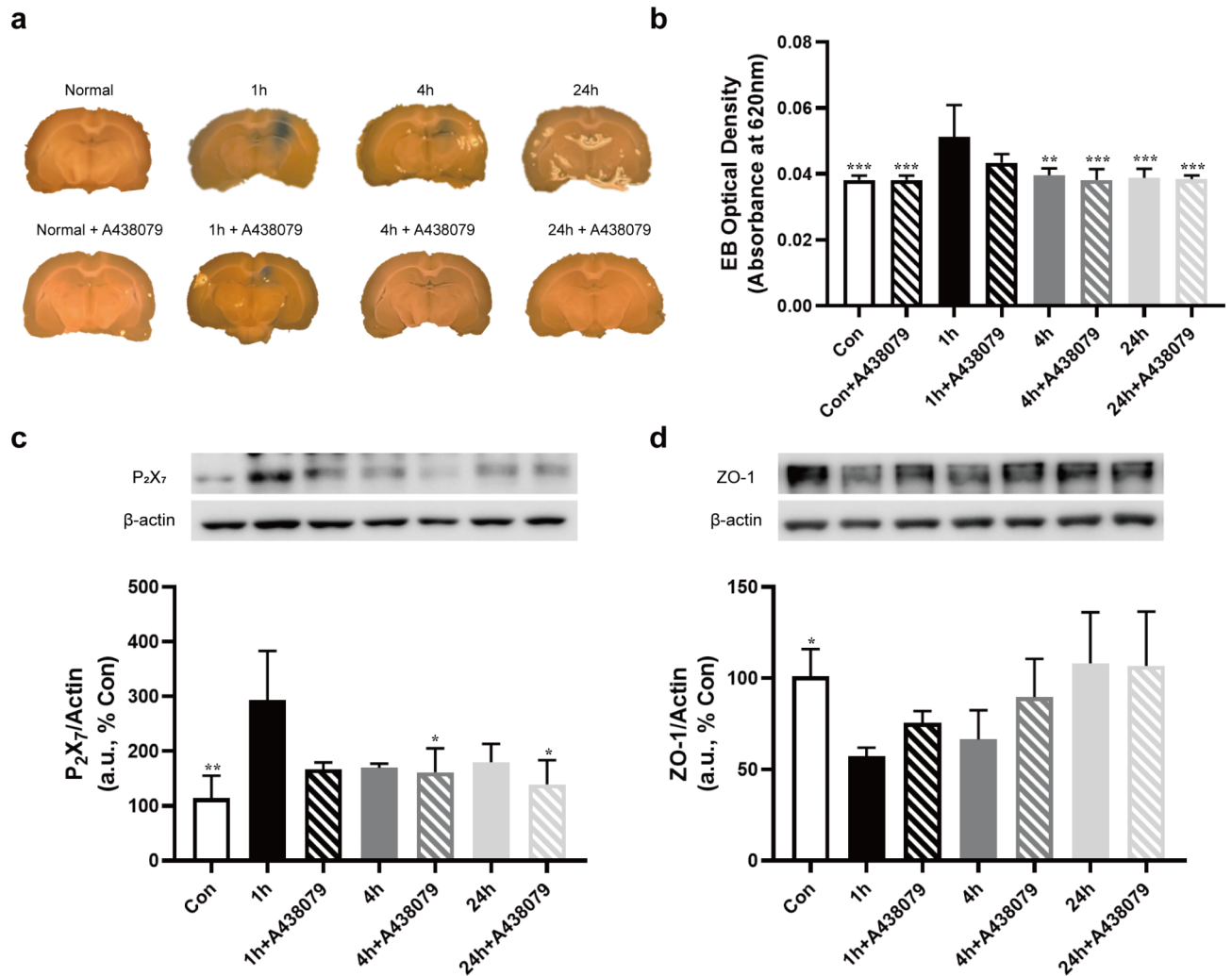


**Fig. 5.** Alterations in BBB permeability following antagonist administration. **(a)** Representative images of Evans blue dye leakage in each group. **(b)** Optical density of Evans blue dye in the sonicated area after LiFUS in each group. \*\*  $p < 0.01$ , \*\*\*  $p < 0.001$ ; compared to 1 h **(c)** Western blot results for the  $P_2X_7$  receptor. The bar graph shows the normalized level of the receptor relative to that of control. Band intensity images for each group are included. \*  $p < 0.05$ , \*\*  $p < 0.01$ ; compared to 1 h. **(d)** Western blot result for ZO-1. The analysis method employed for the ZO-1 was the same as that for the  $P_2X_7$  receptor. No statistical differences were observed among the groups. All data are represented as mean  $\pm$  SD ( $n = 3-5$ ). \*  $p < 0.05$ ; compared to 1 h. One-way ANOVA with Tukey's multiple comparison test was performed.

For a detailed understanding of the leakage phenomenon, we conducted western blot quantification of  $P_2X_7$  and ZO-1 proteins. For the  $P_2X_7$  receptor, the group corresponding to 1 h after LiFUS (1 h:  $293.6 \pm 89.56$ ) exhibited a significant expression level (Fig. 5c, Con:  $114.2 \pm 41.15$ ,  $p < 0.001$ ; 1 h + A438079:  $166.7 \pm 12.79$ ; 4 h:  $170 \pm 7.28$ ; 4 h + A438079:  $161.5 \pm 43.53$ ,  $p < 0.05$ ; 24 h:  $179.9 \pm 33.13$ ; 24 h + A438079:  $139.4 \pm 44.25$ ,  $p < 0.05$  compared to 1 h,  $n = 3-4$  for each group). In contrast, ZO-1 expression was the lowest at 1 h (Fig. 5d, Con:  $104.8 \pm 14.24$   $p < 0.05$  compared to 1 h; 1 h:  $60.37 \pm 7.55$ ; 1 h + A438079:  $80.96 \pm 12.06$ ; 4 h:  $70.24 \pm 15.15$ ; 4 h + A438079:  $84.74 \pm 19.71$ ; 24 h:  $108 \pm 28.08$ ; 24 h + A438079:  $106.7 \pm 29.72$ ,  $n = 3-4$  for each group). The results for the remaining downstream signaling pathways in the antagonist-treated groups are shown in Fig. S3. These findings strongly support a possible role of the  $P_2X_7$  receptor in LiFUS-mediated BBB modulation.

## Discussion

LiFUS has emerged as a promising technique offering the advantage of temporal modulation of the BBB to enhance drug delivery for the treatment of brain diseases<sup>3,17</sup>. Despite its clinical significance, the precise molecular mechanism underlying LiFUS-mediated BBB modulation remains unclear<sup>48-50</sup>. To address this gap and enable the utilization of the LiFUS technique, we sought to demonstrate the involvement of the  $P_2X_7$  receptor in BBB modulation<sup>51-53</sup>. The activation of  $P_2X_7$  receptor and associated factors reached a peak intensity at 1 h after sonication, coinciding with a decrease in tight junction proteins. Notably, there was a substantial disparity



in the extent of dye leakage depending on the presence of  $P_2 \times_7$  receptors. These findings contribute to our understanding of the role of the  $P_2 \times_7$  receptor in LiFUS-mediated BBB modulation<sup>54</sup> (Fig. 6).

Numerous studies have investigated the effects of LiFUS on the BBB<sup>55,56</sup>. Considering the influence of microbubble cavitation, initial observations predominantly focused on sonication-induced alterations in cerebrovascular vessels<sup>57</sup>. Notably, several studies have demonstrated ultrastructural changes in endothelial cell morphology and brain microvessels, suggesting enhanced permeability to macromolecules after LiFUS-induced BBB opening<sup>58</sup>. In addition, analyses of BBB-related proteins have led to the proposal of various possible mechanisms for the passage of substances through the BBB following LiFUS, including paracellular, transcellular, and adsorptive-mediated pathways<sup>59,60</sup>. However, the precise mechanisms underlying BBB modulation are yet to be established.

The present study substantially advances our understanding of the effects of LiFUS. Herein, we demonstrated that LiFUS with microbubbles triggers complex alterations within various neurovascular units, with the  $P_2 \times_7$  receptor acting as a central mediator in this process. The presence of cavitation in both groups 1 h after sonication offers a possible clue. In particular, the differential leakage of Evans blue dye, contingent on the presence of  $P_2 \times_7$  receptors, highlights the multifaceted nature of LiFUS-induced BBB modulation and the significant involvement of the  $P_2 \times_7$  receptors. These data underscore the complexity of LiFUS-induced BBB modulation and the integral role of the  $P_2 \times_7$  receptors in mediating these effects<sup>44</sup>. However, complete restriction of BBB permeability was not achieved even in the antagonist-treated group. Such results are likely due to the involvement of various pathways in LiFUS-induced BBB modulation, as previously suggested<sup>59,60</sup>. Hence, it is necessary to consider the various pathways to gain a comprehensive understanding of BBB modulation.

Moreover, our study provides insight into safety considerations associated with the LiFUS technique. Vigilance is crucial in the post-sonication period to monitor potential edema or hemorrhage resulting from BBB modulation and subsequent inflammatory response at the lesion site. Previous studies have emphasized the sterile inflammatory response, with a focus on alterations in the NF- $\kappa$ B pathway following LiFUS<sup>61,62</sup>. In particular, when quantifying protein levels in the brain following sonication, a transient upregulation of cytokines related to inflammation was observed, which eventually normalized over time<sup>63</sup>. Although the present study revealed similar trends, the outcomes differed significantly. Notably, in our study, the expression of pro-inflammatory cytokines, including NLRP3, IL-1 $\beta$ , and NF- $\kappa$ B, showed an initial increase up to approximately 4 h after sonication. These elevated levels returned to baseline within 24 h. Moreover, TUNEL staining and H&E analysis consistently verified the absence of damage to the brain tissue. Thus, our study demonstrates that LiFUS induces transient alterations in the BBB and its physiology; however, these changes do not reach a critical or injurious threshold. Comparable or milder inflammatory responses have been observed in studies utilizing energy of similar intensity<sup>29,63</sup>. Our findings suggest that LiFUS can be safely applied under well-defined parameters.

We found that the  $P_2 \times_7$  receptors are involved in BBB modulation induced by LiFUS under safe conditions. When applying this technique to patients, the transfer of energy is affected by various parameters, such as individual differences in patient status, even in cases where the inflammatory response needs to be well-controlled, such as in Alzheimer's disease<sup>64,65</sup>. LiFUS energy is applied for a short duration of approximately 2 min. However, the BBB has been shown to be normalized within approximately 1 day<sup>3</sup>. Notably, the BBB opens up approximately 4 h after sonication, allowing continuous drug accumulation in the brain<sup>3,30</sup>. Under such conditions, the extent of BBB tight junction loosening may be regulated by administering  $P_2 \times_7$  receptor antagonists without causing significant damage to the sonicated area, as demonstrated in this study. For the antagonist-treated group (Fig. S3), a slight increase in  $P_2 \times_7$  receptor expression was observed, but it did not show statistical significance, and  $P_2 \times_7$  receptor expression subsequently returned to baseline levels within 24 h. Given the pivotal role of the  $P_2 \times_7$  receptors in brain pathology-related inflammatory pathways, the regulation of receptor activity may serve as a viable approach to attenuate downstream inflammatory processes. Thus, further investigations utilizing  $P_2 \times_7$  antagonists and the optimization of treatment parameters are warranted. Nevertheless, this study serves as a foundational investigation with the potential to expand the scope of existing LiFUS applications.

Although our findings identify potential modulators of LiFUS-mediated BBB opening that can act without causing brain damage, there are some limitations to this study. First, while our study demonstrated  $P_2 \times_7$  receptor activation, which is implicated in BBB modulation, the precise origin of this receptor activation remains unclear<sup>34</sup>. According to previous studies, no significant change was observed in the expression of Iba-1<sup>66</sup> (Fig. S4). Thus, we speculate that the increased expression of  $P_2 \times_7$  receptors may originate from endothelial cells. However, for a more comprehensive understanding, further analyses using techniques such as RNA sequencing should be conducted, particularly considering the clinical applicability of this technology<sup>66,67</sup>. Second, our study focused on analyzing the intracerebral response at an energy level near 0.3 MPa, which translates to approximately 1.6 W/cm<sup>2</sup> in terms of energy per unit area. However, it is important to note that ultrasound energy is employed with a range of powers depending on the specific experimental conditions. Therefore, to assess the effects of LiFUS comprehensively, it is necessary to investigate changes using a broader range of parameters<sup>66,68</sup>. Finally, this study was conducted on rats in a normal physiological state. LiFUS is currently used to treat various brain diseases<sup>69</sup>. It is important to recognize that in diseases that differ from the normal physiological state, the levels of cytokines related to inflammation and biological responses to ultrasound energy may vary<sup>70</sup>. Therefore, the findings of this study should be interpreted with caution. To facilitate a more comprehensive understanding and ensure safer application of this technique, future research should encompass animal models representing diverse brain disease conditions.

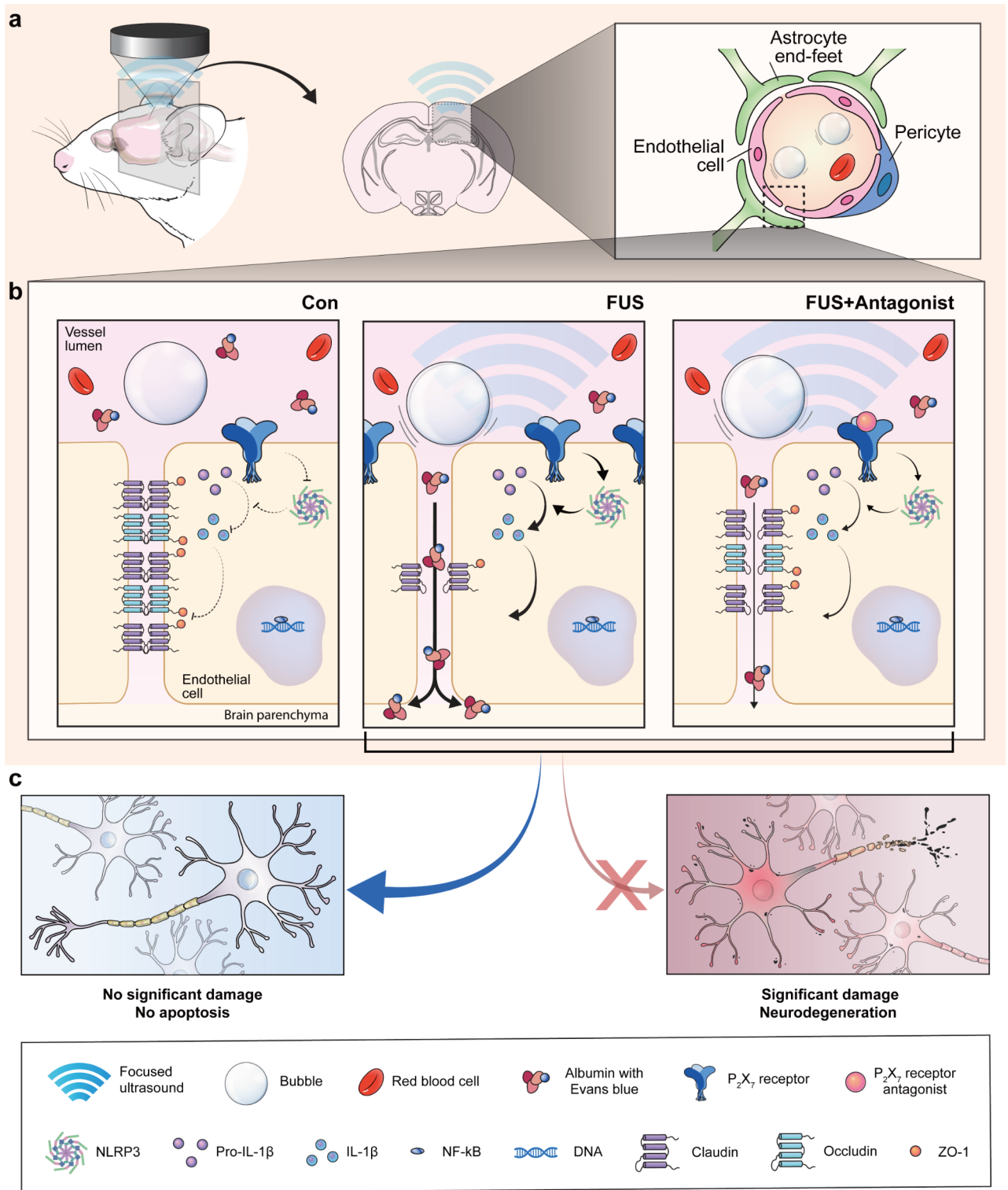


**Fig. 6.** Graphical summary of the study. **(a)** A 0.5-MHz transducer was placed on the skull of rats, and sonication was performed. Microbubbles inside the vessels affected by LiFUS energy loosened the BBB to make it permeable. The hippocampal area was the main region analyzed. **(b)** Compared to the control, in the LiFUS treated group, the upregulated expression of P<sub>2</sub>X<sub>7</sub> receptor, NLRP3, and IL-1 $\beta$  was observed, accompanied by a decrease in the expression level of the tight junction proteins and RNA. Consequently, the leakage of the Evans blue dye in the parenchyma was increased compared to that in the control conditions. In the antagonist-treated group, changes in protein and RNA expression levels were observed, but they did not reach statistical significance. The amount of Evans blue dye leakage was also not significant. **(c)** Although LiFUS induces the temporal upregulation of markers related to the inflammatory responses, including NLRP3, IL-1 $\beta$ , and NF- $\kappa$ B, this technique is safe as it does not reach a level causing cell damage or hemorrhage to the sonicated area.

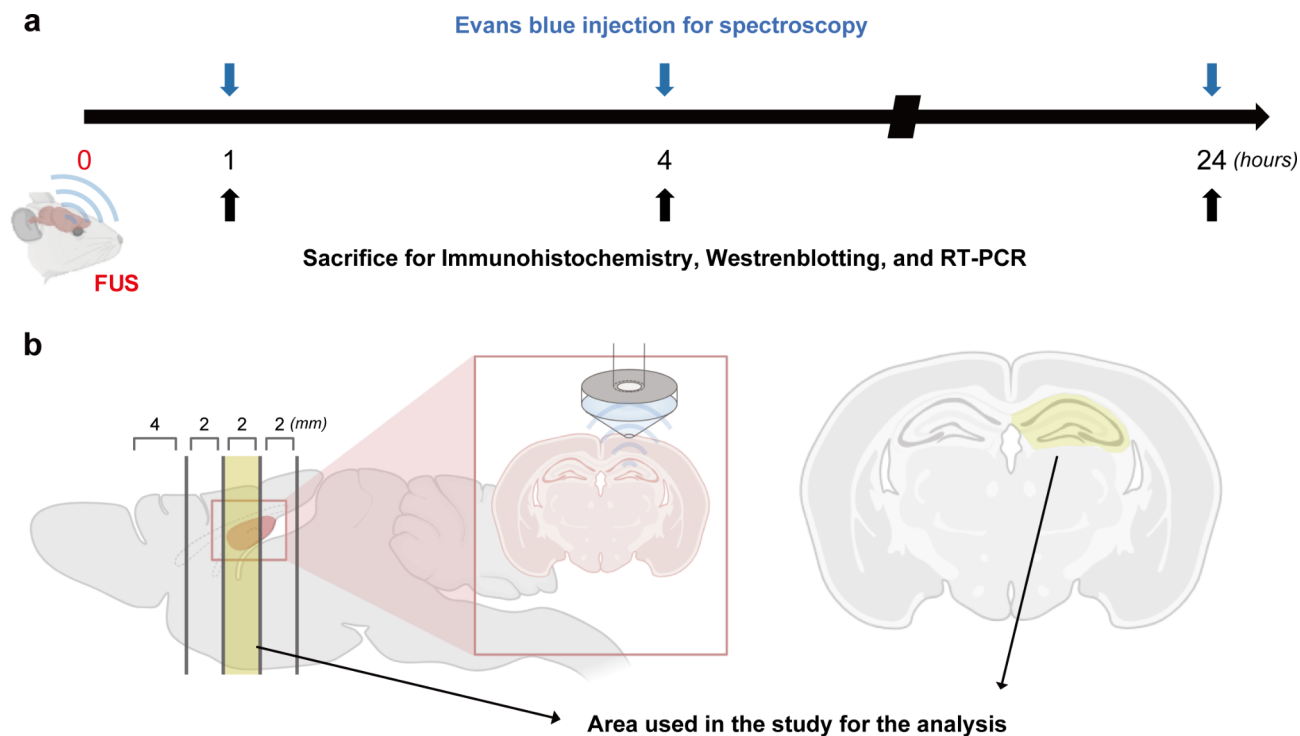


**Fig. 7.** Scheme of the experimental procedure. **(a)** Schematic of the experimental timeline for functional and pathological assessment. **(b)** Schematic region of the study area used for western blotting, IHC, RT-PCR, and Evans blue quantification.

Groups	Con	1 h	4 h	24 h	Total
Sham	8	0	0	0	8
LiFUS only	0	8	8	8	24
LiFUS + antagonist	0	4	4	4	12
LiFUS + Evans blue	5	5	5	5	20
LiFUS + Evans blue + antagonist	5	5	5	5	20

**Table 1.** Number of animals per group.

## Conclusions

Our study confirmed changes in the expression of  $P_2 \times_7$  receptors and BBB-related proteins in response to LiFUS. Furthermore, we demonstrated that the presence or absence of  $P_2 \times_7$  receptors influences the degree of BBB opening. These findings provide valuable insights into the complex mechanisms underlying LiFUS-mediated BBB modulation. Moreover, they support the feasibility of potentially regulating the degree of BBB opening using LiFUS as a noninvasive strategy for modulating the BBB.

## Methods

This study was conducted in accordance with the Guide for the Care and Use of Laboratory Animals of the National Institutes of Health. All animal experiments were approved by Institutional Animal Care and Use Committee (IACUC) of Yonsei University Health System (IACUC #2019–0208) and in compliance with the animal Research: Reporting of In Vivo Experiments (ARRIVE) guidelines. A total of 84 Sprague-Dawley rats (male, 7 weeks old,  $270 \pm 20$  g) were used in this study. Three animals were housed per cage under a light/dark cycle (12 h) in a room with controlled temperature ( $22 \pm 2$  °C) and were allowed free access to food and water. The process and targeted areas for analysis are shown in Fig. 7a and b. The number of animals used in each group is presented in Table 1.

### Low intensity focused ultrasound (LiFUS) treatment with microbubbles in rats

A waveform generator (33220 A, Agilent) was connected to a power amplifier (240 L, ENI Inc.) to facilitate the experimental setup. Subsequently, a coupler (Pulsar C30-102–481/2 N) was used to connect the power amplifier, transducer, and oscilloscope. The 515-kHz single-element transducer (H-107MR, Sonic Concept Inc.) with a full width at half maximum of 4 mm and a focal depth of 51.74 mm was affixed to a custom-designed cone. The tip



of the cone was wrapped in a polyurethane membrane and prefilled with degassed water prior to sonication. The RF signal was monitored continuously using an oscilloscope (DSOX2002A; Keysight Technologies).

Rats were deeply anesthetized via intraperitoneal injection of ketamine cocktail (mixture of 0.9% saline, 75 mg/kg ketamine, 4 mg/kg xylazine and 0.75 mg/kg acepromazine) and positioned in a stereotaxic frame. The scalps of the animals were shaved and subsequently incised, and hemostasis was ensured. To prevent the loss of energy during sonication, an ultrasound transmission gel (ProGel; Dayo Medical Co.) was applied to fill the gap between the animal's skull and the tip of the cone. The target region for sonication was the right hippocampal area, located at coordinates  $-3.5$  mm posterior and 2 mm lateral from the bregma. Intravenous injection of microbubbles in rat's tail (20  $\mu$ L/kg, Definity, Lantheus Medical Imaging) was performed and sonication initiated 10 s after injection. A sonication protocol of approximately 0.3 MPa intensity was employed for each session, with a duration of 2 min, burst duration of 10 ms, and pulse repetition frequency of 1 Hz. Animals were divided into four groups (1, 4, and 24 h after LiFUS and control). The control group did not undergo any sonication procedure.

A specific  $P_2\times_7$  receptor antagonist (A430879, HY-15488; MCE) was diluted in 0.9% normal saline and administered intraperitoneally at a dose of 100 mg /kg per animal 20 min before sonication. Thereafter, identical procedures were performed in all groups.

### Magnetic resonance imaging (MRI)

MRI was performed 1 h after sonication using a Bruker 9.4 T 20-cm bore MRI system (Biospec 94/20 USR; Bruker) and a rat head coil. The animals were anesthetized via inhalation of 2% isoflurane during MRI. A gadolinium-based MRI contrast agent, gadobutrol (Gadovist; 0.2 mL/kg), was injected intravenously, and contrast-enhanced T1-weighted images were used to confirm the opening of the BBB (echo time, 2 ms; repetition time, 8.06 ms; echo train length, 2 ms; slice thickness, 1 mm). For statistical analysis, three rats were included in each study group.

### Immunostaining and histological analyses

Animals were anesthetized with a ketamine cocktail (i.p.) and perfused with 0.9% saline and 4% paraformaldehyde. Subsequently, the brains were collected, fixed in 4% paraformaldehyde for additional 3 days, and then processed for paraffin embedding and sectioning. 5- $\mu$ m tissue sections were de-paraffinized using xylene (UN1307, Duksan) and then rehydrated. The antigen was retrieved using 1 $\times$ citrate buffer 85  $^{\circ}$ C for 15 min. Immunostaining was performed after cooling and rinsing the slides for 20 min. The tissues were blocked for 90 min at room temperature (20  $^{\circ}$ C) using a blocking solution containing phosphate-buffered saline (PBS), 0.2% normal goat serum (S-1000-20, Vector), and 0.2% Triton X-100 (X-100, Sigma Aldrich). Subsequently, the brains were incubated overnight (approximately 16 h) at 4  $^{\circ}$ C in a blocking solution containing anti- $P_2\times_7$  (1:300; ab109054; Abcam), anti-Reca-1 (1:300; ab9774; Abcam), anti-MMP9 (1:300; ab76003; Abcam), anti-MMP2 (1:300; ab92536; Abcam), and anti-Iba-1 (1:500; 019-19741; Wako) antibodies. After the primary immunoreaction, the samples were briefly washed with 1 $\times$  PBS and incubated for 2 h at room temperature with goat anti-rabbit secondary antibodies (1:600; A11008; Thermo Fisher Scientific) conjugated with Alexa Fluor 488 and goat anti-mouse secondary antibodies (1:600; A11005; Thermo Fisher Scientific) conjugated with Alexa Fluor 594. Nuclei were stained with 4',6-diamidino-2-phenylindole (DAPI; 1:1000; D1306; Thermo Fisher Scientific) during conjugation with the secondary antibodies.

Hematoxylin and eosin (H&E) (hematoxylin [ab220365, Abcam] and eosin [ab246824, Abcam]) staining was performed on paraffin sections, and images were acquired using an optical microscope (BX51; Olympus). Histological analysis was performed to examine tissue damage, especially to monitor red blood cell extravasation.

### Western blotting

After anesthesia with ketamine cocktail (i.p.), brains were collected at the indicated time points after LiFUS (1, 4, and 24 h). Samples were homogenized using lysis buffer (PRO-PREP; Intron Biotechnology, Pyeongtaek, Korea) and placed on ice for 30 min, followed by centrifugation at 13,000 rpm for 30 min. The protein concentration in the lysate was measured using the bicinchoninic acid protein assay reagent kit (23227, Thermo Fisher Scientific). Subsequently, 10–20  $\mu$ g of each protein sample were separated via sodium dodecyl sulfate-polyacrylamide gel electrophoresis and transferred to a polyvinylidene fluoride membrane using a Bio-Rad Trans-Blot apparatus. When conducting a western blot with a limited amount of antibody, we cut the PVDF to the size of the gel. Membranes were incubated with blocking buffer (5% nonfat dry milk in PBS containing 0.05% Tween 20 [TBST]) for 1 h at room temperature. The membranes were then incubated with the primary rabbit anti- $P_2\times_7$  (1:1000, ab307718, Abcam), rabbit anti-NLRP3 (1:1000, ab263899, Abcam), rabbit anti-IL-1 $\beta$  (1:1000, NB600-633, Novus Biological), rabbit anti-ZO-1 (1:1000, sc-10804, SantaCruz), rabbit anti-occludin (1:1000, ab216327, Abcam), mouse anti-NF- $\kappa$ B (1:1000, 6956 S, CST), rabbit anti-p-NF- $\kappa$ B (1:1000, 3039 S, CST), rabbit anti-caspase3 (1:1000, 06-735, Millipore), mouse anti-caspase9 (1:1000, 9508 S, CST) and rabbit anti- $\beta$  actin (1:2000, ab8227, Abcam) antibodies overnight (approximately 16 h) at 4  $^{\circ}$ C. Next, the membrane was washed three times for 5 min each and incubated with the corresponding secondary antibodies, either goat anti-rabbit IgG (H + L)-HRP (1:2000, SA002, GenDEPOT) or goat anti-mouse IgG (H + L)-HRP (1:2000, SA001, GenDEPOT), for 90 min at room temperature. Immunoreactive bands were visualized using an enhanced chemiluminescent solution (WEST-Queen; 16026, iNtRON Biotechnology) and developed using LAS 4000 Mini (GE Healthcare Life Sciences). The intensity of each band was determined using an analytical system (MultiGauge version 3.0; Fujifilm).

	Forward sequence	Reverse sequence
P <sub>2</sub> × <sub>7</sub>	CCCTGGCTACAACCTTCAGATACGC	GCTCCACGATGGGCTCACAC
NLRP3	GGGACTCAAGCTCCTCTGTG	GAGGCTCTGGTTATGGGTCA
IL-1β	TGACCCATGTGAGCTGAAAG	AGGGATTTGTGCTTGCTTG
ZO-1	AGACAATAGCATCCTCCCACC	TAGGGTCACAGTGTGGCAAG
Occludin	AACCCGAAGAAAGATGGA	TCTGAAGTGATAGGTGGATA
Caspase3	AGGGGCATGTTTCTGTTTGTG	TTCCAAAACCAGCCTTTGAC
Caspase9	CTGCAGACACCAGCATCACT	CATGTCCTGTTGCCAGTC
MMP2	AAAGGAGGGCTGCATTGTGAA	CTGGGGAAGGACGTGAAGAGG
GAPDH	AGTGCCAGCCTCGTCTCATA	GAAGGGGTCGTTGATGGCAA

**Table 2.** List of primers.

### Quantification of Evans blue dye

Initially, Evans blue dye (E2129, Sigma Aldrich) was diluted to a 2% concentration (g/ml) in 0.9% saline and subsequently prepared by filtering the solution twice. Intravenous injection of diluted Evans blue solution (4 ml/kg) was administered at specific time points (1, 4, and 24 h) after sonication. The dye was allowed to circulate for 1 h prior to further experiments. Subsequently, the rats were perfused with 500 mL saline to remove the dye localized within the intravascular space. The brains were then harvested, coronal sectioned into 2 mm slices and ipsilateral hippocampus was collected within a range of 2–4 mm posterior to the bregma. After weighing, samples were homogenized with saline (mg/ml), and centrifuged at 15,000× g, 4 °C for 30 min to remove tissue debris. 50% trichloroacetic acid (1:3 volume ratio) were added to each supernatant. Samples were incubated at 4 °C overnight and additional centrifuged was performed. To increase their optic length, 90 μL of 95% ethanol was added to each well containing 30 μL supernatant and mixed by repetitive pipetting. The extravasated Evans blue dye was spectrophotometrically quantified at 620 nm/680 nm (excitation/emission wavelength each).

### Real-time reverse transcription-polymerase chain reaction (RT-PCR)

Total RNA was isolated from the cells using an easy-spin total RNA extraction kit (17221, iNtRON Biotechnology), and oligo (dT)-primed cDNA was synthesized from the total RNA using the Maxime RT PreMix kit (25081, iNtRON Biotechnology), according to the manufacturer's instructions. The proteins and each primer used in this study are presented in Table 2. Quantitative RT-PCR was performed using the StepOnePlus real-time PCR system (Thermo Fisher Scientific, Waltham, MA, USA) with the SYBR Green Dye system (SYBR Premix Ex Taq [Tli RNase Plus] and ROX reference dye [TAKARA Bio Inc]). Gene expression level was normalized to glyceraldehyde 3-phosphate dehydrogenase transcript levels.

### Terminal deoxynucleotidyl transferase dUTP nick end labeling (TUNEL) assay

A TUNEL assay kit (G3250, Promega) was used to assess the level of apoptosis in paraffin-embedded rat brain sections according to manufacturer's instructions. Briefly, the paraffin-embedded tissue sections were de-paraffinized, rehydrated, and treated with proteinase K. Permeabilized tissue sections were incubated with the rTdT reaction mixture for 1 h in a dark and humidified chamber at 37 °C. The sections were co-stained with DAPI and cover-slipped with mounting solution. The labeled DNA was observed using an LSM700 confocal microscope (Carl Zeiss). For the brain sections, the detection wavelengths were those of fluorescein isothiocyanate and DAPI.

### ATP assay

An ATP assay kit (ab83355, Abcam) was used to analyze the effects of LiFUS on P<sub>2</sub>×<sub>7</sub>-related ATP levels following the manufacturer's instructions. ATP content was measured using a colorimetric assay, which generated a quantifiable product detected at 570 nm.

### Statistical analysis

For quantitative analysis of Western Blot (WB) and RT-PCR, each data was normalized level of the proteins or RNA with its housekeeping genes. Thereafter, the average value of the control group was calculated, and normalization was subsequently performed by dividing each individual value by this control group average to allow for comparison of expression levels. All results are expressed as the mean ± standard deviation and analyzed using GraphPad Prism 8 (GraphPad Software, Inc.). MATLAB software (R2020b; MathWorks) was used to calculate the intensity of the region of interest (ROI) using the T1 images. Data were analyzed using an unpaired t-test ( $n=3$ ) and one-way analysis of variance, followed by Tukey's post-hoc test ( $n=3-5$ ). P-values lower than 0.05 were considered to indicate statistical significance.

### Data availability

The data presented in this study are available on request from the corresponding authors on reasonable request.

Received: 29 March 2024; Accepted: 18 December 2024

Published online: 06 January 2025

## References

- Ballabh, P., Braun, A. & Nedergaard, M. The blood-brain barrier: an overview: structure, regulation, and clinical implications. *Neurobiol. Dis.* **16**, 1–13. <https://doi.org/10.1016/j.nbd.2003.12.016> (2004).
- Abbott, N. J., Patabendige, A. A., Dolman, D. E., Yusof, S. R. & Begley, D. J. Structure and function of the blood-brain barrier. *Neurobiol. Dis.* **37**, 13–25. <https://doi.org/10.1016/j.nbd.2009.07.030> (2010).
- Greene, C. & Campbell, M. Tight junction modulation of the blood brain barrier: CNS delivery of small molecules. *Tissue Barriers*. **4**, e1138017. <https://doi.org/10.1080/21688370.2015.1138017> (2016).
- Profaci, C. P., Munji, R. N., Pulido, R. S. & Daneman, R. The blood-brain barrier in health and disease: important unanswered questions. *J. Exp. Med.* **217** <https://doi.org/10.1084/jem.20190062> (2020).
- Su, Y. M. & Sinko, P. J. Drug delivery across the blood-brain barrier: why is it difficult? How to measure and improve it? *Expert Opin. Drug Del.* **3**, 419–435. <https://doi.org/10.1517/17425247.3.3.419> (2006).
- Terstappen, G. C., Meyer, A. H., Bell, R. D. & Zhang, W. Strategies for delivering therapeutics across the blood-brain barrier. *Nat. Rev. Drug Discov.* **20**, 362–383. <https://doi.org/10.1038/s41573-021-00139-y> (2021).
- Samanta, S. et al. Exosomes: new molecular targets of diseases. *Acta Pharmacol. Sin.* **39**, 501–513. <https://doi.org/10.1038/aps.2017.162> (2018).
- Hynynen, K., McDannold, N., Vykhotseva, N. & Jolesz, F. A. Noninvasive MR imaging-guided focal opening of the blood-brain barrier in rabbits. *Radiology* **220**, 640–646. <https://doi.org/10.1148/radiol.2202001804> (2001).
- McDannold, N., Vykhotseva, N. & Hynynen, K. Use of ultrasound pulses combined with definity for targeted blood-brain barrier disruption: a feasibility study. *Ultrasound Med. Biol.* **33**, 584–590. <https://doi.org/10.1016/j.ultrasmedbio.2006.10.004> (2007).
- Chang, W. S. et al. Unilateral magnetic resonance guided focused ultrasound thalamotomy for essential tremor: practices and clinicoradiological outcomes. *J. Neurol. Neurosurg. Psychiatry*. **86**, 257–264. <https://doi.org/10.1136/jnnp-2014-307642> (2015).
- Chang, J. W. et al. A prospective trial of magnetic resonance-guided focused Ultrasound Thalamotomy for essential tremor: results at the 2-Year follow-up. *Ann. Neurol.* **83**, 107–114. <https://doi.org/10.1002/ana.25126> (2018).
- Chang, W. S. et al. Factors associated with successful magnetic resonance guided focused ultrasound treatment: efficiency of acoustic energy delivery through the skull. *J. Neurosurg.* **124**, 411–416. <https://doi.org/10.3171/2015.3.Jns142592> (2016).
- Vykhotseva, N., McDannold, N. & Hynynen, K. Progress and problems in the application of focused ultrasound for blood-brain barrier disruption. *Ultrasonics* **48**, 279–296. <https://doi.org/10.1016/j.ultras.2008.04.004> (2008).
- McDannold, N., Vykhotseva, N. & Hynynen, K. Effects of acoustic parameters and ultrasound contrast agent dose on focused-ultrasound induced blood-brain barrier disruption. *Ultrasound Med. Biol.* **34**, 930–937. <https://doi.org/10.1016/j.ultrasmedbio.2007.11.009> (2008).
- Bohmer, M. R. et al. Focused ultrasound and microbubbles for enhanced extravasation. *J. Control Release*. **148**, 18–24. <https://doi.org/10.1016/j.jconrel.2010.06.012> (2010).
- Chen, H. & Konofagou, E. E. The size of blood-brain barrier opening induced by focused ultrasound is dictated by the acoustic pressure. *J. Cerebr Blood F Met.* **34**, 1197–1204. <https://doi.org/10.1038/jcbfm.2014.71> (2014).
- McMahon, D., O'Reilly, M. A. & Hynynen, K. Therapeutic Agent Delivery across the blood-brain barrier using focused Ultrasound. *Annu. Rev. Biomed. Eng.* **23**, 89–113. <https://doi.org/10.1146/annurev-bioeng-062117-121238> (2021).
- Kong, C. et al. Factors Associated with Energy Efficiency of Focused Ultrasound through the Skull: a study of 3D-Printed Skull phantoms and its comparison with clinical experiences. *Front. Bioeng. Biotech.* **9** ARTN 78304810.3389/fbioe.2021.783048 (2021).
- Liu, H. L. et al. Low-pressure pulsed focused ultrasound with microbubbles promotes an anticancer immunological response. *J. Transl Med.* **10**, 221. <https://doi.org/10.1186/1479-5876-10-221> (2012).
- Rezaei, A. R. et al. Noninvasive hippocampal blood-brain barrier opening in Alzheimer's disease with focused ultrasound. *Proc. Natl. Acad. Sci. U S A.* **117**, 9180–9182. <https://doi.org/10.1073/pnas.2002571117> (2020).
- Lipsman, N. et al. Blood-brain barrier opening in Alzheimer's disease using MR-guided focused ultrasound. *Nat. Commun.* **9**, 2336. <https://doi.org/10.1038/s41467-018-04529-6> (2018).
- Gasca-Salas, C. et al. Blood-brain barrier opening with focused ultrasound in Parkinson's disease dementia. *Nat. Commun.* **12**, 779. <https://doi.org/10.1038/s41467-021-21022-9> (2021).
- Chen, P. Y., Wei, K. C. & Liu, H. L. Neural immune modulation and immunotherapy assisted by focused ultrasound induced blood-brain barrier opening. *Hum. Vaccin Immunother.* **11**, 2682–2687. <https://doi.org/10.1080/21645515.2015.1071749> (2015).
- Wang, S. T. et al. Direct brain infusion can be enhanced with focused ultrasound and microbubbles. *J. Cerebr Blood F Met.* **37**, 706–714. <https://doi.org/10.1177/0271678x16637881> (2017).
- Wu, S. K. et al. Characterization of different microbubbles in assisting focused Ultrasound-Induced blood-brain barrier opening. *Sci. Rep.* **7**, 46689. <https://doi.org/10.1038/srep46689> (2017).
- Kong, C. et al. Long-lasting restoration of memory function and hippocampal synaptic plasticity by focused ultrasound in Alzheimer's disease. *Brain Stimul.* **16**, 857–866. <https://doi.org/10.1016/j.brs.2023.05.014> (2023).
- Aryal, M. et al. Effects on P-Glycoprotein expression after blood-brain barrier disruption using focused Ultrasound and Microbubbles. *PLoS One*. **12**, e0166061. <https://doi.org/10.1371/journal.pone.0166061> (2017).
- Kovacs, Z. I., Burks, S. R. & Frank, J. A. Focused ultrasound with microbubbles induces sterile inflammatory response proportional to the blood brain barrier opening: attention to experimental conditions. *Theranostics* **8**, 2245–2248. <https://doi.org/10.7150/thno.24181> (2018).
- McMahon, D., Poon, C. & Hynynen, K. Evaluating the safety profile of focused ultrasound and microbubble-mediated treatments to increase blood-brain barrier permeability. *Expert Opin. Drug Deliv.* **16**, 129–142. <https://doi.org/10.1080/17425247.2019.1567490> (2019).
- Tung, Y. S., Vlachos, F., Feshitan, J. A., Borden, M. A. & Konofagou, E. E. The mechanism of interaction between focused ultrasound and microbubbles in blood-brain barrier opening in mice. *J. Acoust. Soc. Am.* **130**, 3059–3067. <https://doi.org/10.1121/1.3646905> (2011).
- Park, S. H. et al. Extensive frontal focused ultrasound mediated blood-brain barrier opening for the treatment of Alzheimer's disease: a proof-of-concept study. *Transl Neurodegener.* **10**, 44. <https://doi.org/10.1186/s40035-021-00269-8> (2021).
- Albalawi, F. et al. The P2X7 Receptor Primes IL-1beta and the NLRP3 Inflammasome in Astrocytes Exposed to Mechanical Strain. *Front. Cell. Neurosci.* **11**, 227. <https://doi.org/10.3389/fncel.2017.00227> (2017).
- Miras-Portugal, M. T. et al. P2X7 receptors in the central nervous system. *Biochem. Pharmacol.* **187**, 114472. <https://doi.org/10.1016/j.bcp.2021.114472> (2021).
- Yu, Y. et al. Cellular localization of P2X7 receptor mRNA in the rat brain. *Brain Res.* **1194**, 45–55. <https://doi.org/10.1016/j.brainres.2007.11.064> (2008).
- Di Virgilio, F., Ben, D., Sarti, D., Giuliani, A. C., Falzoni, S. & A. L. & The P2X7 Receptor in Infection and Inflammation. *Immunity* **47**, 15–31. <https://doi.org/10.1016/j.immuni.2017.06.020> (2017).
- Illes, P., Verkhatsky, A., Burnstock, G. & Franke, H. P2X receptors and their roles in Astroglia in the Central and Peripheral Nervous System. *Neuroscientist* **18**, 422–438. <https://doi.org/10.1177/1073858411418524> (2012).
- Monif, M., Reid, C. A., Powell, K. L., Smart, M. L. & Williams, D. A. The P2X7 receptor drives microglial activation and proliferation: a trophic role for P2X7R pore. *J. Neurosci.* **29**, 3781–3791. <https://doi.org/10.1523/JNEUROSCI.5512-08.2009> (2009).
- Burnstock, G. Purinergic signalling and disorders of the central nervous system. *Nat. Rev. Drug Discov.* **7**, 575–590. <https://doi.org/10.1038/nrd2605> (2008).



39. Burnstock, G. An introduction to the roles of purinergic signalling in neurodegeneration, neuroprotection and neuroregeneration. *Neuropharmacology* **104**, 4–17. <https://doi.org/10.1016/j.neuropharm.2015.05.031> (2016).
40. Kara, A. & Ozkanlar, S. Blockade of P2X7 receptor-mediated purinergic signaling with A438079 protects against LPS-induced liver injury in rats. *J. Biochem. Mol. Toxicol.* **37**, e23443. <https://doi.org/10.1002/jbt.23443> (2023).
41. Le Dare, B. et al. Ethanol upregulates the P2X7 purinergic receptor in human macrophages. *Fundam Clin. Pharmacol.* **33**, 63–74. <https://doi.org/10.1111/fcp.12433> (2019).
42. Wang, K. F. et al. The improvement of Sepsis-Associated Encephalopathy by P2X7R inhibitor through inhibiting the Omi/HtrA2 apoptotic signaling pathway. *Behav. Neurol.* **2022** Artn 3777351.1155/2022/3777351 (2022).
43. Zhao, H. et al. P2X7 Receptor Suppression Preserves Blood-Brain Barrier through Inhibiting RhoA Activation after Experimental Intracerebral Hemorrhage in Rats. *Sci. Rep.* **6**, 23286. <https://doi.org/10.1038/srep23286> (2016).
44. Qu, Y. & Dubyak, G. R. P2X7 receptors regulate multiple types of membrane trafficking responses and non-classical secretion pathways. *Purinerg Signal.* **5**, 163–173. <https://doi.org/10.1007/s11302-009-9132-8> (2009).
45. Manaka, S. et al. Low-intensity pulsed ultrasound-induced ATP increases bone formation via the P2X7 receptor in osteoblast-like MC3T3-E1 cells. *FEBS Lett.* **589**, 310–318. <https://doi.org/10.1016/j.febslet.2014.12.013> (2015).
46. Yang, F., Zhao, K., Zhang, X., Zhang, J. & Xu, B. ATP Induces Disruption of Tight Junction Proteins via IL-1 Beta-Dependent MMP-9 Activation of Human Blood-Brain Barrier In Vitro. *Neural Plast* 8928530, doi: (2016). <https://doi.org/10.1155/2016/8928530> (2016).
47. Wang, H. L. & Lai, T. W. Optimization of Evans blue quantitation in limited rat tissue samples. *Sci. Rep.* **4**, 6588. <https://doi.org/10.1038/srep06588> (2014).
48. Man, V. H. et al. Molecular mechanism of ultrasound interaction with a blood brain barrier model. *J. Chem. Phys.* **153**, 045104. <https://doi.org/10.1063/5.0010667> (2020).
49. Cho, H. et al. Localized down-regulation of P-glycoprotein by focused Ultrasound and Microbubbles induced blood-brain barrier disruption in rat brain. *Sci. Rep.* **6**, 31201. <https://doi.org/10.1038/srep31201> (2016).
50. Jalali, S., Huang, Y. X., Dumont, D. J. & Hynynen, K. Focused ultrasound-mediated bbb disruption is associated with an increase in activation of AKT: experimental study in rats. *Bmc Neurol* **10**, doi:Artn 11410.1186/1471-2377-10-114 (2010).
51. Jiang, L. H., Baldwin, J. M., Roger, S. & Baldwin, S. A. Insights into the molecular mechanisms underlying mammalian P2X7 receptor functions and contributions in diseases, revealed by structural modeling and single nucleotide polymorphisms. *Front Pharmacol* **4**, doi:ARTN 5510.3389/fphar.00055 (2013). (2013).
52. Browne, L. E., Compan, V., Bragg, L. & North, R. A. P2X7 receptor channels allow direct permeation of nanometer-sized dyes. *J. Neurosci.* **33**, 3557–3566. <https://doi.org/10.1523/JNEUROSCI.2235-12.2013> (2013).
53. Komalavilas, P. et al. Vascular surgical stretch injury leads to activation of P2X7 receptors and impaired endothelial function. *PLoS One.* **12**, e0188069. <https://doi.org/10.1371/journal.pone.0188069> (2017).
54. Calzaferrri, F. et al. Synthesis and Pharmacological Evaluation of Novel Non-nucleotide Purine Derivatives as P2X7 Antagonists for the Treatment of Neuroinflammation. *J. Med. Chem.* **64**, 2272–2290. <https://doi.org/10.1021/acs.jmedchem.0c02145> (2021).
55. Poon, C., Pellow, C. & Hynynen, K. Neutrophil recruitment and leukocyte response following focused ultrasound and microbubble mediated blood-brain barrier treatments. *Theranostics* **11**, 1655–1671. <https://doi.org/10.7150/thno.52710> (2021).
56. Todd, N. et al. Secondary effects on brain physiology caused by focused ultrasound-mediated disruption of the blood-brain barrier. *J. Control Release.* **324**, 450–459. <https://doi.org/10.1016/j.jconrel.2020.05.040> (2020).
57. Raymond, S. B., Skoch, J., Hynynen, K. & Bacskai, B. J. Multiphoton imaging of ultrasound/Optison mediated cerebrovascular effects in vivo. *J. Cereb. Blood Flow. Metab.* **27**, 393–403. <https://doi.org/10.1038/sj.jcbfm.9600336> (2007).
58. Urban, A. et al. Understanding the neurovascular unit at multiple scales: advantages and limitations of multi-photon and functional ultrasound imaging. *Adv. Drug Deliver Rev.* **119**, 73–100. <https://doi.org/10.1016/j.addr.2017.07.018> (2017).
59. Deng, J. et al. The role of caveolin-1 in blood-brain barrier disruption induced by focused ultrasound combined with microbubbles. *J. Mol. Neurosci.* **46**, 677–687. <https://doi.org/10.1007/s12031-011-9629-9> (2012).
60. Pandit, R. et al. Role for caveolin-mediated transcytosis in facilitating transport of large cargoes into the brain via ultrasound. *J. Control Release.* **327**, 667–675. <https://doi.org/10.1016/j.jconrel.2020.09.015> (2020).
61. Shih, R. H., Wang, C. Y. & Yang, C. M. NF-kappaB Signaling pathways in neurological inflammation: a Mini Review. *Front. Mol. Neurosci.* **8**, 77. <https://doi.org/10.3389/fnmol.2015.00077> (2015).
62. Thawkar, B. S. & Kaur, G. Inhibitors of NF-kappaB and P2X7/NLRP3/Caspase 1 pathway in microglia: Novel therapeutic opportunities in neuroinflammation induced early-stage Alzheimer's disease. *J. Neuroimmunol.* **326**, 62–74. <https://doi.org/10.1016/j.jneuroim.2018.11.010> (2019).
63. Kovacs, Z. I. et al. Disrupting the blood-brain barrier by focused ultrasound induces sterile inflammation. *Proc. Natl. Acad. Sci. U S A.* **114**, E75–E84. <https://doi.org/10.1073/pnas.1614777114> (2017).
64. Wasielewska, J. M. & White, A. R. Focused Ultrasound-mediated drug delivery in humans - a path towards translation in neurodegenerative diseases. *Pharm. Res.* **39**, 427–439. <https://doi.org/10.1007/s11095-022-03185-2> (2022).
65. Souza, R., da Silva, I. C. S., Delgado, A. B. T., da Silva, P. H. V. & Costa, V. R. X. focused ultrasound and Alzheimer's disease A systematic review. *Dement. Neuropsychol.* **12**, 353–359. <https://doi.org/10.1590/1980-57642018dn12-040003> (2018).
66. Choi, H. J. et al. The new insight into the inflammatory response following focused ultrasound-mediated blood-brain barrier disruption. *Fluids Barriers Cns.* **19** <https://doi.org/10.1186/s12987-022-00402-3> (2022).
67. Ji, R. et al. Cavitation-modulated inflammatory response following focused ultrasound blood-brain barrier opening. *J. Control Release.* **337**, 458–471. <https://doi.org/10.1016/j.jconrel.2021.07.042> (2021).
68. Han, M., Seo, H., Choi, H., Lee, E. H. & Park, J. Localized Modification of Water Molecule Transport after focused Ultrasound-Induced blood-brain barrier disruption in rat brain. *Front. Neurosci.* **15**, 685977. <https://doi.org/10.3389/fnins.2021.685977> (2021).
69. Mishra, A. et al. P2X7 receptor in multifaceted cellular signalling and its relevance as a potential therapeutic target in different diseases. *Eur. J. Pharmacol.* **906** ARTN 17423510.1016/j.ejphar.2021.174235 (2021).
70. Noel, R. L. et al. Natural aging and Alzheimer's disease pathology increase susceptibility to focused ultrasound-induced blood-brain barrier opening. *Sci. Rep.* **13**, 6757. <https://doi.org/10.1038/s41598-023-30466-6> (2023).

## Acknowledgements

We thank the Medical Illustration & Design (MID) team in the Medical Research Support Services of Yonsei University College of Medicine for their excellent support with the medical illustrations and figures made on Biorender.com.

## Author contributions

Y.C.N., J.L., and B.W.S. conceptualized and designed the study. J.L., Y.S., J.P., H.K., and S.H. assisted with and performed experiments. J.P. Y.C.N., B.W.S. and W.S.C. analyzed the data. W.S.C., Y.C.N., B.W.S., and J.P. edited the manuscript. J.P. and Y.C.N. wrote the original draft. All the authors have read and approved the final version of the manuscript.

## Funding

This study was funded by the Basic Science Research Program of the National Research Foundation (NRF) of Korea supported by the Ministry of Education [2019R1I1A3A01043477, RS-2023-00266075] and the Korea government (MSIT) [NRF-2020R1C1C1013535].

## Declarations

### Competing interests

The authors declare no competing interests.

### Ethics approval

All animal experiments were conducted in accordance with the Institutional Animal Care and Use Committee (IACUC) of Yonsei University Health System (IACUC #2019 – 0208).

### Additional information

**Supplementary Information** The online version contains supplementary material available at <https://doi.org/10.1038/s41598-024-83913-3>.

**Correspondence** and requests for materials should be addressed to B.-W.S. or W.S.C.

**Reprints and permissions information** is available at [www.nature.com/reprints](http://www.nature.com/reprints).

**Publisher's note** Springer Nature remains neutral with regard to jurisdictional claims in published maps and institutional affiliations.

**Open Access** This article is licensed under a Creative Commons Attribution-NonCommercial-NoDerivatives 4.0 International License, which permits any non-commercial use, sharing, distribution and reproduction in any medium or format, as long as you give appropriate credit to the original author(s) and the source, provide a link to the Creative Commons licence, and indicate if you modified the licensed material. You do not have permission under this licence to share adapted material derived from this article or parts of it. The images or other third party material in this article are included in the article's Creative Commons licence, unless indicated otherwise in a credit line to the material. If material is not included in the article's Creative Commons licence and your intended use is not permitted by statutory regulation or exceeds the permitted use, you will need to obtain permission directly from the copyright holder. To view a copy of this licence, visit <http://creativecommons.org/licenses/by-nc-nd/4.0/>.

© The Author(s) 2024